Description of Libra Files and Post-Processors:

AOS Safety Analysis Report

Prepared for: GE-Hitachi Nuclear Energy
PO No. 431004505
May 3, 2007

Prepared by: Structural Mechanics Analysis, Inc.
P.O. Box 700910
San Jose, CA 95170-0910

0.1 Table of Contents

0.2 List of Figures

1.0 Introduction

The Alpha-Omega Services (AOS) Safety Analysis Report (SAR) applies to four radioactive materials Type B cask configurations. These four cask configurations are designated by their relative size as AOS-025, AOS-050, AOS-100, and AOS-165. Configuration AOS-025 is approximately 25% the size of configuration AOS-100, configuration AOS-050 approximately 50%, and configuration AOS-165 approximately 165% in comparison to the AOS-100 model. The following provides a description of the Libra post-processors used to perform the structural and thermal analyses to support the preparation of the SAR for the four AOS cask models.

Notwithstanding the scaled nature of the four configurations, the thermal and stress analyses for the four models are not scalable. Rather, an independent set of analyses is required for each model. While the analyses are not scalable, the finite element models used in the analyses are largely scaled, although there are significant differences between models, particularly between model AOS-165 and the others.

Almost all of the thermal and stress analyses in the SAR are based on application of the Structural Mechanical Analysis, Inc. (SMA) Libra finite element program. The Libra program has been used by GE-Hitachi Nuclear Energy Americas, LLC ("GEH") for a number of years, and was used in the licensing of the Model 2000 Type B transport packaging. SMA has proprietorship of the Libra program, as a result, SMA was able to develop sophisticated post-processing tools integrated with the Libra program, that facilitated the AOS analyses.

The majority of the SAR analyses permit use of axisymmetric, finite element models, since for the majority of load cases the cask, loading, and boundary conditions are axisymmetric. As a result, four axisymmetric models were developed corresponding to the four cask configurations, and these models are the cornerstones of all the finite element analyses in the SAR. For load cases such as drop and transport, where assumptions of axisymmetric loading and boundary conditions are not applicable, 3D finite element models are used. These 3D models are generated from the axisymmetric models by rotation of the model. In this way, there is a well-defined relationship between elements in the axisymmetric and 3D models, and this relationship allows combining stress resultants from the two models.

The two U.S. Nuclear Regulatory Commission (NRC) documents that govern the analyses included in the SAR are Regulatory Guides 7.6 and 7.8. Reg. Guide 7.6 defines the allowable stresses for nuclear shipping casks, while Reg. Guide 7.8 defines the required loading conditions and load combinations. Further, Reg. Guide 7.6 specifies allowable stresses in terms of membrane and bending stresses, or more generally stress resultants. Stress resultants are not a direct output of finite element analyses. For the detailed models used in the AOS analyses, forming stress resultants involves identifying and integrating element stresses across a number selected cask cross-sections. This is an arduous and time consuming task. In addition, NRC Reg. Guide 7.8, which defines the load combinations that must be meet, presents additional difficult tasks for analyses based on the finite element method.

Two major post-processing programs were developed to facilitate evaluation of stress resultants and stress combinations required by NRC Reg. Guides 7.6 and 7.8. The first, PmPb, forms the stress resultants required by Reg. Guide 7.6, while the second, CmbLds, forms the load combinations required by Reg. Guide 7.8. The methodology and application of these programs are described in detail in this report. The solution process for all of the four cask configurations involves first finding stresses corresponding to a set of basic load conditions, and then finding the stress combinations. For thermal loading conditions, one or more thermal solutions must be found before solving for stresses. After determining load case stresses, stress resultants are formed by application of the PmPb post-processing program. The PmPb program generates files containing stress resultants for the basic loading conditions. After all of the loading conditions have been run, and corresponding files of stress resultants generated by PmPb, The CmbLds program is executed. The CmbLds program reads the files generated by PmPb, forms the required combinations, and compares the combined stresses to the allowables in Reg. Guide 7.6. This entire process is automated by a Windows Command program, Run_AOS. A section of the Run_AOS batch program is shown in Appendix F.

2.0 PmPb Post Processor Program

The PmPb program forms the stress resultants referenced by Reg. Guide 7.6. The PmPb is a suite of three programs: PmPbData, PmPb, and PmPb3D. Each of these thee programs is described below. All three programs use the input file PmPb.in, which lists the elements at each model cross-section where stress resultants are evaluated. A sample PmPb.in file is shown in Appendix A.

The cross-sections on which PmPb operates are shown in Figures 1 and 2. Figure 1 shows the cross-sections for model 165, and Figure 2 shows the cross-section for models 025, 050, and 100. Model 165 has 25 stress cross-sections, while models 025,050, and 100 have 22 stress cross-sections. The larger number of cross-sections for model 165 is due to the split outer shell. The elements comprising the cross-sections shown in Figures 1 and 2 are defined on the respective input data file PmPb.dat. The 165 cask axisymmetric, and three dimensional finite element models are shown in Figures 3 and 4, respectively.

2.1 AOS Input Load Case designations

AOS Libra input data files all have designations starting with LCnnn, where nnn is a three digit load case number; and ending with suffix mmm, where mmm is a three digit model number. For example, the input file for thermal load case 101, model 025 is, LC101.025. Additional file description is entered following the load case number, with a hyphen preceding the entry. For example LC101-2500-UPDATE.025 is the designation for input file for thermal load case 101, 2500 watts, updated.

AOS load case numbers define the type of loading involved in the load case. Load cases numbered 101-199 are thermal loadings. Load cases 201-299 are pressure or other axisymmetric normal loadings. Load cases 301-399 are accident condition loadings. The load case types are used by the CmbLds program to determine allowable stress for load combinations.

2.2 PmPbData Program

PmPbData program determines the geometry data for the PmPb program, and stores this data on the file PmPb.dat. This geometry function is separated from the PmPb program for efficiency, as it needs to be performed only once for each model. PmPbData must be executed immediately following an execution of the Libra program, as it uses Libra output. The program reads Libra model geometry data from binary file Tape9, and generates the geometric data required to form membrane and moment stress resultants for each stress cross-section. This data is written to the file PmPb.dat, and is utilized by both PmPb and PmPb3D.

2.3 PmPb Program

The PmPb program generates files of membrane and bending stress resultants for axisymmetric loading conditions. The program utilizes the geometry data on the file PmPb.dat, the cross-section elements defined on PmPb.in, and Libra stress data on the binary file Tape8. PmPb generates output files labeled LOAD_CASE.nnn, where nnn is the load case number. For each LCnnn file there is a corresponding LOAD_CASE.nnn file. A typical output file generated by PmPb is shown in Appendix B. Output files list maximum principal stress, and membrane and bending stress for each cross-section. The PmPb program must be executed immediately following execution of a Libra stress run.

2.4 PmPb3D Program

The PmPb3D program generates files containing membrane and moment stress resultants for 3D loading conditions. The program utilizes the geometry data on the file PmPb.dat, cross-section element data on the file PmPb.in, and Libra stress output on the binary file Tape8. All AOS 3D models are generated from axisymmetric models. As a result, each element along a meridian corresponds to a element in the corresponding axisymmetric model. PmPb3D finds the stress resultants for each element along a meridian, and outputs maximum values on the LOAD_CASE file. Stress combinations involving axisymmetric and 3D load cases conservatively combine maximum meridian 3D values with axisymmetric values. The output of PmPb3D is the same as PmPb, and a typical file shown in Appendix B.

2.5 GroupAllow Program

The GroupAllow program finds maximum temperatures at cross-sections where stress resultants are evaluated, and interpolates temperature-dependent, allowable stress data to find the allowable cross-section stress corresponding to these maximum temperatures. This program is executed only for thermal load cases, and is executed after a Libra thermal solution. The GroupAllow program generates files ALLOWABLES.nnn, where nnn is load case number, and the file is subsequently used by the CmbLds program. A typical GroupAllow output file is shown in Appendix C.

3.0 CmbLds Program

As described in Section 2.3, The PmPb program generates stress resultant files LOAD_CASE.nnn, where nnn is the load case number. The CmbLds program forms load combinations using these files, and also determines the allowable stresses against which the combined stresses are compared. A typical CmbLds.in file is shown in Appendix D.

The load case number nnn in the file name LOAD_CASE.nnn defines the type of loading, as described in Section 2.1. LOAD_CASE.nnn files list both membrane and bending stress for each stress cross-section. The ALLOWABES.nnn files, described in Section 2.5, specify allowable stresses for thermal loadings. Based on all this information, the CmbLds program determines the maximum combined stress, the minimum allowable stress, and the minimum margin of safety at all stress cross-sections. The maximum stresses and minimum allowables are output on the file CmbLds.out. A typical output section generated by CmbLds is shown in Appendix E. The table in Appendix E lists the combined stress, allowable stress, and minimum margins of safety for each cross-section. The overall minimum margin of safety is listed at the end of the table.

4.0 AOS Files

The AOS input and output data files, PMPB verification files, and Libra Program files are contained on a single CD. The folders on this disk are listed below, and the following sections describe the contents of these folders.

aos-25	Input data files for AOS cask Model 025
aos-50	Input data files for AOS cask Model 050
aos-100	Input data files for AOS cask Model 100
aos-165	Input data files for AOS cask Model 165
aos-165-2500	Input data files for AOS cask Model 165, 2500 watts
PMPB_Verification	Verification report for post-processors
Source	Post-processors source code
aos-25-out	Output files for AOS cask Model 025
aos-50-out	Output files for AOS cask Model 050
aos-100-out	Output files for AOS cask Model 100
aos-165-out	Output files for AOS cask Model 165
aos-165-2500-out	Output files for AOS cask Model 165, 2500 watts
drop-25	Files for AOS cask Model 025 30' drop analyses
drop-50	Files for AOS cask Model 050 30' drop analyses
drop-100	Files for AOS cask Model 100 30' drop analyses
drop-165	Files for AOS cask Model 165 30' drop analyses

4.1 Input Data Files

The five input data folders, aos-25 ... aos-165-2500, contain all files required to run the Libra stress and thermal analyses for the five cask models. After establishing the Libra program (see Section 4.5), there is a two step process for executing Libra analyses and post-processing programs for a cask model: 1) copy the entire contents of an input data folder onto the Libra.app, or Libra.app sub-folder, directory; 2) execute the batch program RUN_AOS.

All input data is in English units. For thermal problems temperatures are in degrees F, energy in Btu, and length in inches. For structural problems loads are in lb, moduli in lb/in^2, and length in inches.

Libra executions may take several hours. Output from the Libra runs and post-processors consist of a series of text files labeled Load_Case.nnn, where nnn represents the load case number, and a file labeled Cmb_Loads.out. The Load_Case.nnn files contain the Pm and Pb stress measures at the monitored cask cross-sections for the individual load cases. The Cmb_Loads.out file contains the load combination results, including margins of safety for all combined load cases.

4.2 PMPB Verification Files

The PMPB_Verification folder contains both a report and a verification problem for PMPB and Cmb_Loads post-processors. The verification problem is a simple flat-top cylindrical shell under pressure and thermal loads. The stress resultants as two shell cross-sections are determined analytically, and by the PMPB and Cmb_Loads post processors. The two sets of results are shown to compare well.

A folder containing a set of verification problems for the Libra program, with emphasis on the AOS problem types, is established with installation of the Libra program (see Section 4.5). The Source folder contains the Fortran source codes for the six post processing programs used in the AOS Libra analyses.

4.3 Output Data Files

The AOS-25-out ... AOS-165-2500-out folders contain selected output from the individual Libra load case analyses (see Section 2.1). Each folder contains the LOAD_CASE file (see Section 2.4), The ALLOWABLES file (see Section 2.5), and the Libra output file (TAPE6) for each input data file. The extensions on LOAD_CASE, ALLOWABLES, and TAPE6 files are the same as the input file extension.

4.4 Files for 30' Drop Analyses

The four drop analysis folders, drop-25 ... drop-165, contain input and selected output files for the 30' head-on, side and cg/corner drop analyses. Each folder contains files for a single model, and for the three drop analyses. The output files are plot files for force-energy curves, model displacement, and model stress. The file names have -force,- disp, or -stress to indicate content. File names containing -cold are plots for -40° F thermal conditions, all other files are for 75° F.

The same Libra input data file can be used for all three drop orientations, with non-applicable orientation data commented out by an asterisk in column 1. All of the plot files are BMP format files, and may be viewed by means of the MS Paint program. The displacement and stress files are for displacement fields close to, but not necessarily at maximum values.

The drop-165 folder also contains the Libra input data file slap-down.t5 for slap-down analysis. This file is specifically for AOS model 165 cask, but is easily adapted to other cask models by changing the model structure dimensions and contact stiffness values. Contact stiffness values are taken from the 30' side-drop analyses.

5.0 Libra Installation

Libra installation files are contained in the Libra64 folder. The Libra Program is installed by executing the SETTUP program on the Libra64 folder. The SETUP program will request names for Libra Program and Application directories. Libra program files reside on the Program directory, and problems are executed from the Application directory or sub-directories. Default folder names are Libra64 for the program directory, and Libra.app for the application directory. The SETUP program will also prompt for installation of the 64-bit version of Libra. The 64-bit version should be installed only if the host operating system is 64 bits.

On Vista operating systems it may be necessary to set permission for running Script files before executing the Libra SETUP program. The following steps establish permission:

go to Control Panel
click on User Accounts
click on Turn user control on or off
uncheck user account control

After the Libra SETUP program is completed, the Libra program can be executed from the Start menu, or from the Command line in the Libra application folder. The AOS files are organized to run from the Libra Command line. To access the Libra Command line, left click on the Libra Desktop icon. To then execute a Libra input file, at the Command prompt enter,

Libra input_file output_file

If output_file is omitted, the default file name is TAPE6. After a Libra execution, the model can be viewed by entering HPLOT at the command prompt, and stresses viewed by entering STRSPP. Both HPLOT and STRSPP are menu driven.

To execute a set of AOS analyses on the distribution disk, say \aos-25, read the entire contents of \aos-25 onto the application directory (or sub-directory), then enter run_aos at the Command prompt. This executes the batch program run_aos, which executes all of the files and post-processors for AOS Model 025. Output will be contained on a set of files labeled Load_Case.nnn, and on the file Cmb_Loads.out (see Sections 2.3 and 3.0).

Libra installation establishes a folder labeled Verification. This folder contains a number of verification problems for Libra elements and solution procedures. The thermal problems, and several of the structural problems are directly applicable to AOS analyses. In total, the verification problems in this folder encompass all of the Libra elements and solution procedures applied in the AOS analyses. The verification files described in Section 4.2 address the post-processors used in the AOS analyses, and are an adjunct to these Libra verification problems.

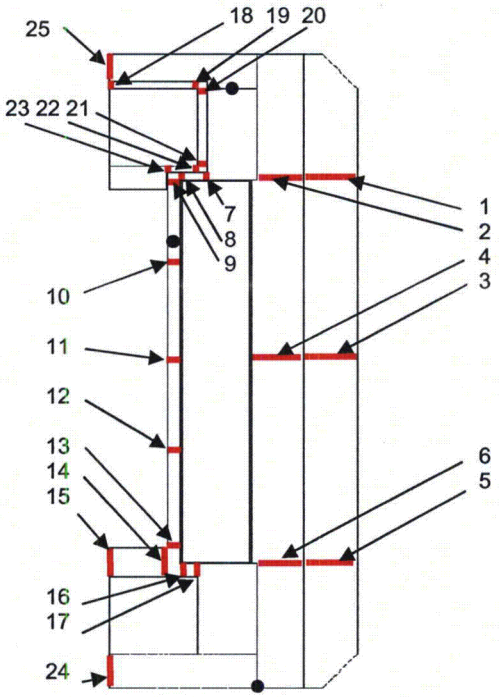

Figure 1. Model 165 PmPb Cross-Sections

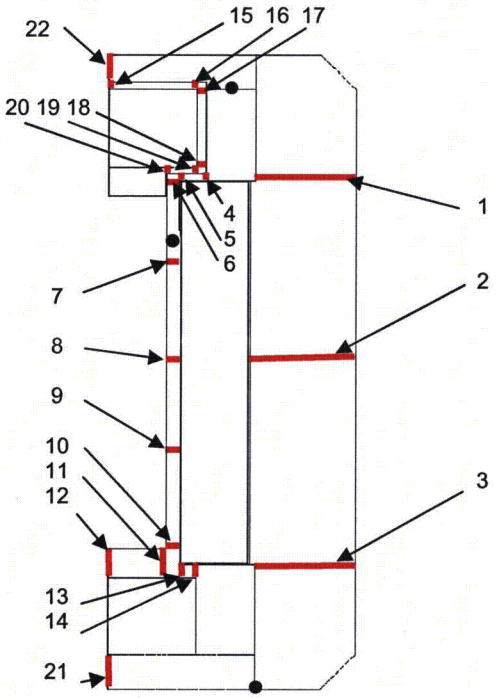

Figure 2. Models 025, 050 and 100 PmPb Cross-Sections

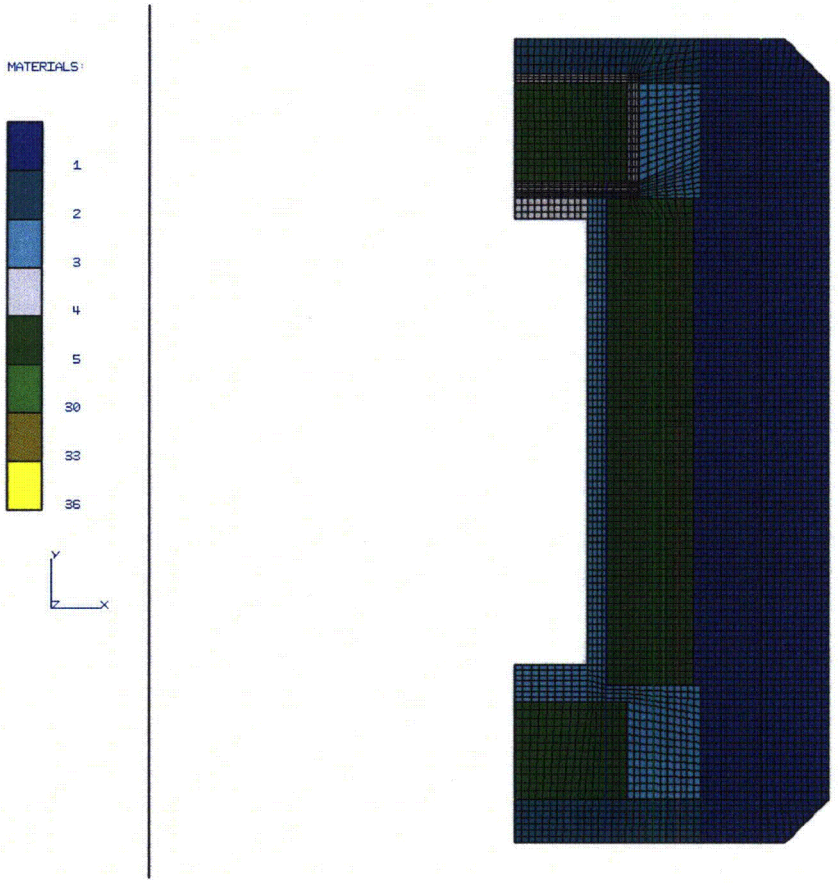

Figure 3. Axisymmetric FEA Model of 165 Cask

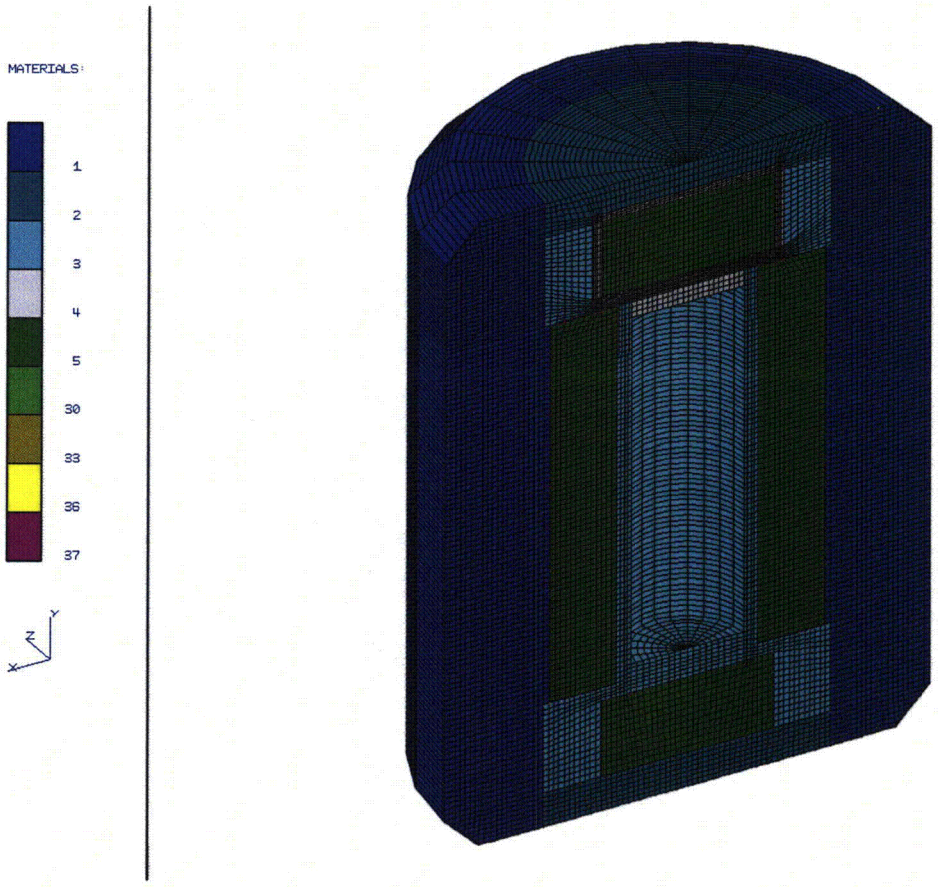

Figure 4. Three Dimensional FEA Model of 165 Cask

Appendix A. Typical PmPb.in File

The following is a typical PmPb.in file listing elements at each stress cross-section. For ease of viewing, cross-section entries are not confined to one line, and blank lines separate entries. In the actual file all section entries are on one line, and there are no blank lines.

```
1957,1958,1959,1960,1961,1962,1963,1964,1965,2146,2147,2148,2149,2150,
2151,2152,2153,2154,2155

552,904,905,906,907,908,909,910,911,912,1587,1588,1589,1590,1591,1592,
1593,1594,1595,1596

348,349,350,351,352,353,354,355,356,507,508,509,510,511,512,513,514,515,
516

4587,4591,4595,4599

4572,4575,4578,4581

552,4553,4554,4555

4476,4477,4478,4479

4408,4409,4410,4411

4344,4345,4346,4347

4280,4281,4282,4283

4141,4150,4159,4168,4177,4186,4195

4133,4142,4151,4160,4169,4178,4187

4212,4215,4218,4221

4214,4217,4220,4223

5218,5236,5254

5235,5253,5271

5214,5215,5216,5217

5166,5167,5168,5169

5140,5143,5146,5149

5122,5126,5130,5134

3001,3017,3033,3049,3065,3081,3097

3190,3208,3226,3244
```

Appendix B. PmPb output file, LOAD_CASE.101

The following is the PmPb output file for load case LC101.025. The file lists maximum principal stresses, and calculated membrane and bending stress at each section analyzed. Stresses are listed in both English and metric units.

Load Case_101 - 100F Ambient, Max Decay Heat

Stress (psi/MPa)

Location	Sigma_1	Sigma_2	Sigma_3	Pm	Pb
1	1.2232E+01	-2.5191E+01	-1.8387E+00	3.7423E+01	5.8177E+01
	8.4340E-02	-1.7369E-01	-1.2677E-02	2.5803E-01	4.0111E-01
2	1.6225E+01	-3.2962E+01	-6.5255E+00	4.9187E+01	1.0016E+02
	1.1187E-01	-2.2727E-01	-4.4992E-02	3.3913E-01	6.9059E-01
3	1.0870E+01	-2.3382E+01	-1.1174E+00	3.4252E+01	5.3526E+01
	7.4943E-02	-1.6122E-01	-7.7043E-03	2.3616E-01	3.6905E-01
4	6.2382E+01	-2.3843E+02	-4.1530E+01	3.0081E+02	5.9563E+02
	4.3011E-01	-1.6439E+00	-2.8634E-01	2.0740E+00	4.1067E+00
5	6.1432E+01	-2.6905E+02	-1.2242E+02	3.3048E+02	5.2038E+02
	4.2356E-01	-1.8550E+00	-8.4406E-01	2.2786E+00	3.5879E+00
6	6.4534E+00	-1.3381E+02	-1.5795E+02	1.4026E+02	1.6725E+02
	4.4494E-02	-9.2256E-01	-1.0890E+00	9.6705E-01	1.1532E+00
7	-1.9752E+00	-4.9672E+01	2.5928E+00	4.7697E+01	4.3899E+01
	-1.3619E-02	-3.4248E-01	1.7877E-02	3.2886E-01	3.0267E-01
8	-2.0037E+00	-4.9648E+01	1.9949E-03	4.7644E+01	4.3457E+01
	-1.3815E-02	-3.4231E-01	1.3755E-05	3.2850E-01	2.9962E-01
9	-1.9811E+00	-4.9582E+01	-5.2273E-01	4.7600E+01	4.1764E+01
	-1.3659E-02	-3.4185E-01	-3.6041E-03	3.2819E-01	2.8795E-01
10	-7.5888E+00	-6.6970E+01	1.0700E+01	5.9381E+01	1.2009E+02
	-5.2323E-02	-4.6174E-01	7.3772E-02	4.0942E-01	8.2802E-01
11	-1.6114E+01	-1.0104E+02	-5.3150E+01	8.4930E+01	7.0193E+00
	-1.1110E-01	-6.9668E-01	-3.6645E-01	5.8557E-01	4.8396E-02
12	4.9440E+00	-1.1870E+02	-1.1938E+02	1.2364E+02	7.5796E+00
	3.4087E-02	-8.1839E-01	-8.2311E-01	8.5248E-01	5.2260E-02

13	-1.3346E+01	-1.7829E+02	-2.9776E+01	1.6495E+02	8.7679E+01
	-9.2016E-02	-1.2293E+00	-2.0530E-01	1.1373E+00	6.0452E-01
14	-1.2832E+01	-1.5680E+02	3.6799E+00	1.4396E+02	9.5911E+01
	-8.8473E-02	-1.0811E+00	2.5372E-02	9.9259E-01	6.6128E-01
15	3.4752E+02	-3.2306E+02	-3.0278E+01	6.7058E+02	1.1250E+03
	2.3960E+00	-2.2274E+00	-2.0876E-01	4.6235E+00	7.7568E+00
16	1.2110E+02	-2.3963E+02	-7.8259E+01	3.6074E+02	5.8708E+02
	8.3498E-01	-1.6522E+00	-5.3958E-01	2.4872E+00	4.0478E+00
17	5.3313E+01	-1.6483E+02	7.7898E+00	2.1815E+02	3.7767E+02
	3.6758E-01	-1.1365E+00	5.3709E-02	1.5041E+00	2.6039E+00
18	1.3652E+01	-8.6978E+01	1.2149E+02	1.0063E+02	1.5144E+02
	9.4130E-02	-5.9969E-01	8.3767E-01	6.9382E-01	1.0442E+00
19	3.7352E+01	-1.4759E+02	9.9594E+01	1.8495E+02	3.1090E+02
	2.5754E-01	-1.0176E+00	6.8668E-01	1.2752E+00	2.1436E+00
20	2.5189E+01	-1.9576E+02	9.1481E+00	2.2095E+02	4.1088E+02
	1.7367E-01	-1.3497E+00	6.3074E-02	1.5234E+00	2.8329E+00
21	6.6491E+00	-2.2294E+00	-1.0467E+00	8.8785E+00	6.0550E+00
	4.5844E-02	-1.5371E-02	-7.2168E-03	6.1215E-02	4.1748E-02
22	2.7655E+00	-1.5235E+01	-3.0961E+00	1.8000E+01	4.4221E+01
	1.9068E-02	-1.0504E-01	-2.1347E-02	1.2411E-01	3.0489E-01

Appendix C. GroupAllow Program Output File

The following is the GroupAllow program output file for load case LC101.025. This file lists maximum and average temperatures at each stress section, and the allowable membrane, yield, and ultimate stress at these sections.

Allowable Stress for Load Case 101

LOC	Tmax (deg_F)	Tave (deg_F)	Sm (ksi)	Sy (ksi)	Su (ksi)
1	138.91	138.74	20.00	30.00	70.00
2	138.94	138.59	20.00	30.00	70.00
3	138.62	138.37	20.00	30.00	70.00
4	139.15	139.13	20.00	30.00	70.00
5	139.61	139.54	20.00	30.00	70.00
6	139.79	139.72	20.00	30.00	70.00
7	140.04	139.89	20.00	30.00	70.00
8	139.99	139.85	20.00	30.00	70.00
9	139.92	139.77	20.00	30.00	70.00
10	139.78	139.64	20.00	30.00	70.00
11	139.92	139.66	20.00	30.00	70.00
12	140.39	140.09	20.00	30.00	70.00
13	139.33	139.20	20.00	30.00	70.00
14	139.04	138.97	20.00	30.00	70.00
15	139.08	139.03	20.00	30.00	70.00
16	139.19	139.14	20.00	30.00	70.00
17	139.22	139.19	20.00	30.00	70.00
18	139.37	139.34	20.00	30.00	70.00
19	139.50	139.44	20.00	30.00	70.00
20	140.26	140.14	20.00	30.00	70.00
21	138.43	138.36	20.00	30.00	70.00
22	138.82	138.76	20.00	30.00	70.00

Appendix D. Typical CmbLds.in File

The following is a typical PmPb.in file. The first entry is the number of stress cross-sections. The next set of entries is the load case numbers, and this set is terminated with a -1. The second and last set of entries are the load combination numbers, and the combination load cases. Text following entries is descriptive, and not used by the program

```
22
101       ; 100F Ambient, Max Decay Heat
102       ; 100F Ambient, Max Decay Heat, Max Insolation
103       ; -20F Ambient, Zero Decay Heat, Zero Insolation
104       ; -40F Ambient, Zero Decay Heat, Zero Insolation
105       ; -40F Ambient, Max Decay Heat
111       ; Fire @ 30 Min, 1475F Ambient, Max Decay Heat
112       ; Fire @60 Min, 100F, Max Decay Heat,Max Insolation
113       ; Fire @90 Min, 100F, Max Decay heat,Max Insolation
114       ; Fire @120 Min, 100F, Max Decay Heat,Max Insolation
115       ; Fire @150 Min, 100F, Max Decay Heat,Max Insolation
116       ; Fire @180 Min, 100F, Max Decay Heat,Max Insolation
201       ; Maximum Internal Pressure, 30 psi
202       ; Minimum External Pressure, 3.5 psia
203       ; Maximum Increased Pressure, 20 psia
204       ; Additional Increased External Pressure, 290 psi
211       ; Fabrication Stress
215       ; Compression Load
216       ; Rod Drop
221       ; Forward 5g Vibration Inertia Load
222       ; Lateral 5g Vibration Inertia Load
223       ; Vertical 10g Vibration Inertia Load
231       ; 4 ft head-on drop
232       ; 30 ft head-on drop, normal conditions
301       ; 30 ft Head-on drop
302       ; 30 ft Side drop + slap-down
303       ; CG/Corner Drop
304       ; 30 ft Head-on drop, low temp
305       ; 30 ft Side drop + slap-down, low temp
306       ; CG/Corner Drop, low temp
311       ; 3 ft drop onto rod
-1
101, 101,201,211          ; hot environment
102, 104,201,211          ; cold environment
103, 103,201,211          ; increaded ex pres
104, 101,201,202,211      ; min ex pres
105, 105,201,202,211      ; cold environment
106, 101,201,203,211      ; max pres, hot environment
107, 105,201,203,211      ; max pres, cold environment
215, 215,101,201,211      ; compression load
216, 216,101,201,211      ; rod drop
217, 216,104,201,211      ; rod drop cold environment
221, 221,101,201,211      ; fwd vibration
222, 222,101,201,211      ; lateral vibration
```

```
223, 223,101,201,211     ; vertical vibration
231, 231,102,201,211     ; 4 ft head-on drop, normal conditions
232, 232,102,201,211     ; 30 ft head-on drop, normal conditions
301, 301,102,201,211     ; head-on drop
302, 302,102,201,211     ; side drop
303, 303,102,201,211     ; cg/corner drop
304, 304,105,202,211     ; head-on drop, cold environment
305, 305,105,202,211     ; side drop, cold environment
306, 306,105,202,211     ; cg/corner drop, cold environment
310, 204,101,211         ; add ext pres (290 psi)
311, 311,101,201,211     ; 3 ft drop onto rod
312, 311,104,201,211     ; 3 ftdrop onto rod, cold environment
350, 111,201,211         ; fire @ 30 min
351, 112,201,211         ; fire @ 60 min
352, 113,201,211         ; fire @ 90 min
353, 114,201,211         ; fire @ 120 min
354, 115,201,211         ; fire @ 150 min
355, 116,201,211         ; fire @ 180 min
-1
```

Appendix E. Typical Output from CmbLds Program

The following is a typical output file from the CmbLds program. The load combination is listed at the top of the table. The file lists maximum membrane and bending stress, and minimum allowables at each section analyzed. Stresses are listed in both English and metric units. Minimum MS and associated values are listed at the end of the table.

```
Normal Load Combination  101
----------------------------
Load Cases: 101 201 211
100F Ambient, Max Decay Heat
Maximum Internal Pressure - 30 Psia
Fabrication Stress
```

	Stress (ksi/MPa)							
Loc	Pm	Pb	Q	Pm+Pb	Pm+Pb+Q	Sm	Su	MS
1	0.75	1.10	0.04	1.85	1.89	20.00	70.00	>10
	5.16	7.60	0.26	12.75	13.01	137.90	482.63	
2	0.14	0.20	0.05	0.34	0.38	20.00	70.00	>10
	0.96	1.35	0.34	2.31	2.65	137.90	482.63	
3	0.08	0.08	0.03	0.16	0.20	20.00	70.00	>10
	0.58	0.54	0.24	1.12	1.36	137.90	482.63	
4	1.16	1.78	0.30	2.94	3.24	20.00	70.00	9.20
	8.00	12.28	2.07	20.28	22.35	137.90	482.63	
5	1.18	1.00	0.33	2.18	2.51	20.00	70.00	>10
	8.17	6.88	2.28	15.05	17.32	137.90	482.63	
6	0.78	1.17	0.14	1.95	2.09	20.00	70.00	>10
	5.40	8.05	0.97	13.44	14.41	137.90	482.63	
7	0.34	0.07	0.05	0.40	0.45	20.00	70.00	>10
	2.34	0.45	0.33	2.79	3.12	137.90	482.63	
8	0.32	0.04	0.05	0.36	0.41	20.00	70.00	>10
	2.21	0.27	0.33	2.48	2.81	137.90	482.63	
9	0.36	0.07	0.05	0.43	0.48	20.00	70.00	>10
	2.48	0.48	0.33	2.97	3.29	137.90	482.63	
10	1.23	0.15	0.06	1.38	1.44	20.00	70.00	>10
	8.49	1.03	0.41	9.52	9.93	137.90	482.63	

11	0.93	1.23	0.08	2.17	2.25	20.00	70.00	>10
	6.44	8.51	0.59	14.95	15.53	137.90	482.63	
12	1.01	1.49	0.12	2.50	2.62	20.00	70.00	>10
	6.95	10.27	0.85	17.23	18.08	137.90	482.63	
13	1.19	1.05	0.16	2.24	2.40	20.00	70.00	>10
	8.21	7.23	1.14	15.44	16.58	137.90	482.63	
14	1.21	1.54	0.14	2.75	2.89	20.00	70.00	9.91
	8.36	10.61	0.99	18.97	19.96	137.90	482.63	
15	1.70	1.94	0.67	3.64	4.31	20.00	70.00	7.25
	11.69	13.38	4.62	25.07	29.70	137.90	482.63	
16	1.70	2.69	0.36	4.39	4.75	20.00	70.00	5.83
	11.72	18.55	2.49	30.27	32.75	137.90	482.63	
17	1.12	1.79	0.22	2.90	3.12	20.00	70.00	9.33
	7.71	12.31	1.50	20.02	21.52	137.90	482.63	
18	0.87	1.40	0.10	2.27	2.37	20.00	70.00	>10
	5.99	9.65	0.69	15.64	16.33	137.90	482.63	
19	1.46	2.17	0.18	3.63	3.82	20.00	70.00	7.26
	10.09	14.96	1.28	25.05	26.33	137.90	482.63	
20	1.82	2.90	0.22	4.72	4.95	20.00	70.00	5.35
	12.58	19.99	1.52	32.57	34.09	137.90	482.63	
21	0.32	0.44	0.01	0.76	0.77	20.00	70.00	>10
	2.24	3.00	0.06	5.24	5.30	137.90	482.63	
22	0.46	0.47	0.02	0.93	0.95	20.00	70.00	>10
	3.20	3.23	0.12	6.43	6.55	137.90	482.63	

Min MS: 5.350, Location: 20, Combination: Pm+Pb

Appendix F. Typical Section of Batch Program to Execute AOS Load Cases

The AOS input data files and post-processor executions are organized and run by a Command batch program. A separate batch program is required for each of the four model configurations. A section of a typical batch program is shown below. Note that the program PmPbData is run before the first execution of PmPb. The GroupAllow program is only run after a Libra thermal analysis. The PmPb (or PmPb3D) program is run after each Libra stress analysis. Calls to the Libra program include the input file name, output file name, and a flag set to 1 to prevent Libra pausing after execution.

```
rem load case 101
call libra lc101-t-update.025  tape6 1
call libra lc101-update.025  tape6 1
groupallow lc101-update.025
pmpbdata
pmpb

rem load case 102
call libra lc102-t-update.025  tape6 1
call libra lc102-update.025  tape6 1
groupallow lc102-update.025
pmpb

rem load case 103
call libra lc103-t-update.025  tape6 1
call libra lc103-update.025  tape6 1
groupallow lc103-update.025
pmpb

rem load case 104
call libra lc104-t-update.025  tape6 1
call libra lc104-update.025  tape6 1
groupallow lc104-update.025
pmpb

rem load case 105
call libra lc105-t-update.025  tape6 1
call libra lc105-update.025  tape6 1
groupallow lc105-update.025
pmpb

rem load case 106
call libra lc106-t-update.025  tape6 1
call libra lc106-update.025  tape6 1
groupallow lc106-update.025
pmpb
```

THIS PAGE INTENTIONALLY LEFT BLANK

2.12.5 Selected Material Properties References

This appendix provides information related to the following materials, that is not included elsewhere in the SAR:

- Contact Resistance
- Decay Heat
- Structural Stability
- Tungsten Alloy
- General Plastics LAST-A-FOAM
- Cask Lid Elastomeric Seal and Port Seal

THIS PAGE INTENTIONALLY LEFT BLANK

Contact Resistance

THIS PAGE INTENTIONALLY LEFT BLANK

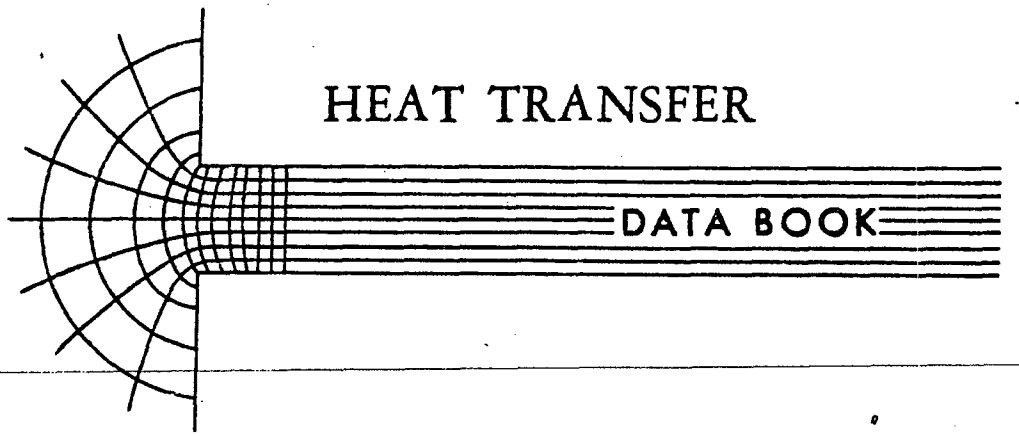

EDITORS	TENURE AS EDITOR
R. Hosmer Norris	1943 - 1971
Mrs. Florence F. Buckland	1943 - 1963
Mrs. Nancy D. Fitzroy	1956 -

GENERAL ELECTRIC COMPANY
CORPORATE RESEARCH AND DEVELOPMENT
Schenectady, N.Y.

GENERAL ELECTRIC

STEEL, BARE SURFACES AT HIGH CONTACT PRESSURES (0 to 1200 psi) - Solid blocks in air at reduced pressure ($p < 0.1$ atm)

For steel with bare surfaces in air, see pages 5-6.
For steel with sandwich material in air, see page 8.
For steel in other gases, see page 9.
For steel with dissimilar metal in air, see page 20; at reduced pressure ($p < 0.1$ atm), see page 21.
For other metals in air, see pages 10-11, 17; at reduced pressure ($p < 0.1$ atm), see pages 12-13, 18-19.
For laminated steels in air, see page 23.

Curve	Material[4]	Finish	Roughness Rms (μ in.) Block 1	Roughness Rms (μ in.) Block 2	Fluid in Gap	Temp (°F)	Condition	Ref. No.[4]
a	Stainless Steel 304	Ground	42-60	43-48	Air	75	Clean, 10^{-4} mm Hg abs	45
b	Stainless Steel 304	Ground	15-15	10-10	Air	84	Clean, 10^{-4} mm Hg abs	45

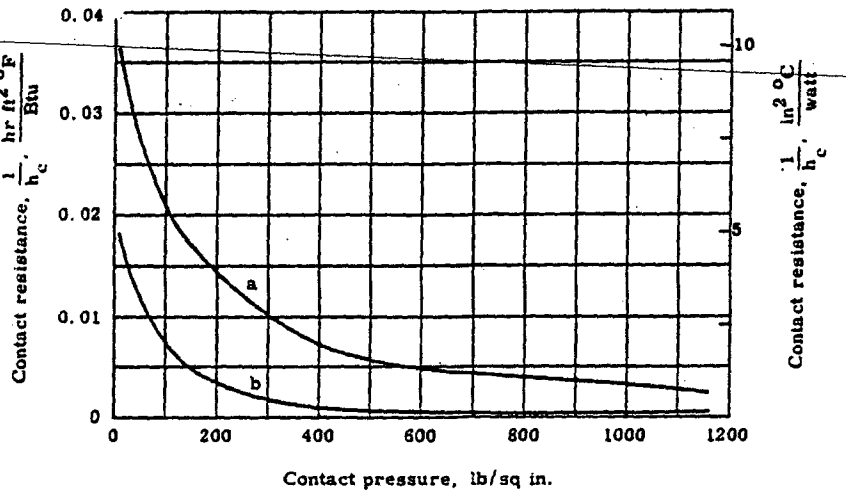

[4-5] See page 24

Decay Heat

Decay Heat Load

Model AOS-025 Cask

Decay Heat = 10W

$$10W = 3.4121 * 10 = 34.121 \text{ Btu/hr}$$

Cavity Area

$$A = 2\pi (0.812^2 + (0.612)(7.0 - 2.0))$$

$$= 29.65 \text{ in}^2$$

Heat Flux

$$q = 341.21 / 29.65$$

$$= 1.151 \text{ Btu/hr-in}^2$$

Model AOS-050 Cask

Decay Heat = 100W

$$100W = 3.4121 * 100 = 341.21 \text{ Btu/hr}$$

Cavity Area

$$2\pi (1.62424^2 + 1.62424 * (14.0 - 4.0))$$

$$= 118.63 \text{ in}^2$$

Heat Flux

$$341.21 / 118.63 = 2.876 \text{ Btu/hr-in}^2$$

Model AOS-100 Cask

Outside Cask Body and Cask Height – Model AOS-100

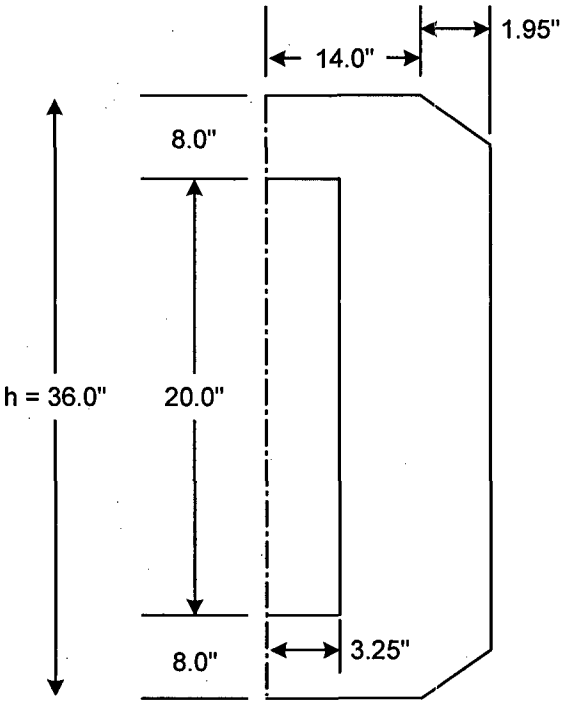

Decay Heat = 400W

400W = 3.4121 * 400 = 1,365 Btu/hr

Cavity Surface Area

$2\pi (3.25^2 + ((3.25)(20))) = 474.77 \text{ in}^2$

Heat Flux

$1{,}365 / 474.77 \text{ in}^2 = 2.88 \text{ Btu/hr-in}^2$

THIS PAGE INTENTIONALLY LEFT BLANK

Structural Stability

THIS PAGE INTENTIONALLY LEFT BLANK

INTRODUCTION TO
Structural Stability Theory

GEORGE GERARD, Sc.D.

Associate Director of Research and
Research Professor of Aeronautics
College of Engineering, New York University

McGRAW-HILL BOOK COMPANY, INC. 1962

New York *Toronto* *London*

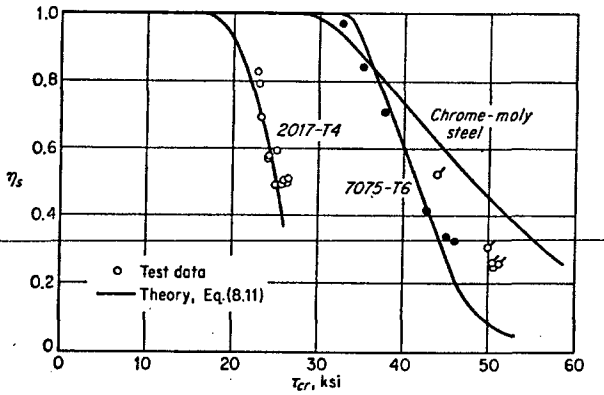

FIG. 8.4. Comparison of test data with plasticity-reduction factor for long cylinders in torsion.

In Fig. 8.3, test data (summarized in Ref. 8.2) on failure of cylinders in torsion of several materials are presented and compared with theory. It can be observed that the upper limit of the test data does conform to the theory. As a result of the postbuckling behavior of cylinders in torsion, there is a considerable mass of test data that lie somewhat below the theory. On the whole, the average of the test data is approximately 15 per cent below theory in the moderate-length-cylinder range.

Before discussing the discrepancy for the torsion case any further, it is convenient to consider the axial compressive buckling of cylinders. Certain additional principles have been evolved in connection with the compressive case that are useful in discussing the small discrepancy between theory and test data in the torsion case (Sec. 8.7).

For torsional loadings, inelastic stability of moderate-length and long cylinders has been considered in Ref. 8.4, and the following plasticity-reduction factor has been derived:

$$\eta_s = \left(\frac{1 - \nu_e^2}{1 - \nu_p^2}\right)^{3/4} \frac{E_s}{E} \tag{8.11}$$

A comparison of Eq. (8.11) with test data summarized in Ref. 8.6 on several materials is presented in Fig. 8.4. Agreement between test data and theory is particularly good for the two aluminum alloys.

8.4. Elastic Stability under Compression

For a circular cylinder under axial compression, $N_{xy} = N_y = 0$, $N_x = \sigma t$, and therefore the governing equilibrium relation [Eq. (7.33)]

reduces to

$$D\nabla^8 w + \sigma t \nabla^4 \frac{\partial^2 w}{\partial x^2} + \frac{Et}{R^2}\frac{\partial^4 w}{\partial x^4} = 0 \tag{8.12}$$

A solution of Eq. (8.12) that satisfies the boundary conditions of simple support at the ends of the cylinder is

$$w = w_{mn} \sin \frac{m\pi x}{L} \sin \frac{ny}{R} \tag{8.13}$$

Upon substituting the appropriate derivatives of Eq. (8.13) into (8.12), the following nontrivial solution is obtained:

$$\sigma_{cr} = \frac{\pi^2 k_c E}{12(1-\nu^2)}\left(\frac{t}{L}\right)^2 \tag{8.14}$$

where

$$k_c = \frac{(m^2+\beta^2)^2}{m^2} + \frac{12Z^2m^2}{\pi^4(m^2+\beta^2)^2} \tag{8.15}$$

$$\beta = \frac{nL}{\pi R}$$

It can be observed that the wavelength parameter $(m^2+\beta^2)^2/m^2$ appears in both terms of Eq. (8.15). By minimizing Eq. (8.15) with respect to this parameter, we obtain

$$\frac{(m^2+\beta^2)^2}{m^2} = \left(\frac{12Z^2}{\pi^4}\right)^{1/2} \tag{8.16}$$

Substituting into Eq. (8.15), we obtain the solution for a moderate-length cylinder under compression:

$$k_c = 0.702Z \tag{8.17}$$

By substituting Eq. (8.17) into (8.14), we obtain the simple result

$$\sigma_{cr} = CE\frac{t}{R} \tag{8.18}$$

where

$$C = [3(1-\nu^2)]^{-1/2} \cong 0.6$$

We return now to Eq. (8.16) to establish the range of validity of Eqs. (8.17) and (8.18). By solving Eq. (8.16) for β, we obtain

$$\beta = \left[\frac{(12Z^2)^{1/4}}{\pi}m - m^2\right]^{1/2} \tag{8.19}$$

Since, as a minimum, $m = 1$, it is apparent that for real values of β

$$Z \geq \frac{\pi^2}{12^{1/2}} \geq 2.85 \tag{8.20}$$

Thus, the moderate-length-cylinder solution applies for values of Z greater than 2.85.

Short Cylinders

For short cylinders of Z less than 2.85, the values of $\beta = 0$ and $m = 1$ are to be substituted into Eq. (8.15). Thus, for a simply supported cylinder in the short-cylinder range,

$$k_c = 1 + \frac{12Z^2}{\pi^4} \tag{8.21}$$

In this region, the short cylinder behaves in the same manner as a wide, simply supported column which buckles into one half-wave-

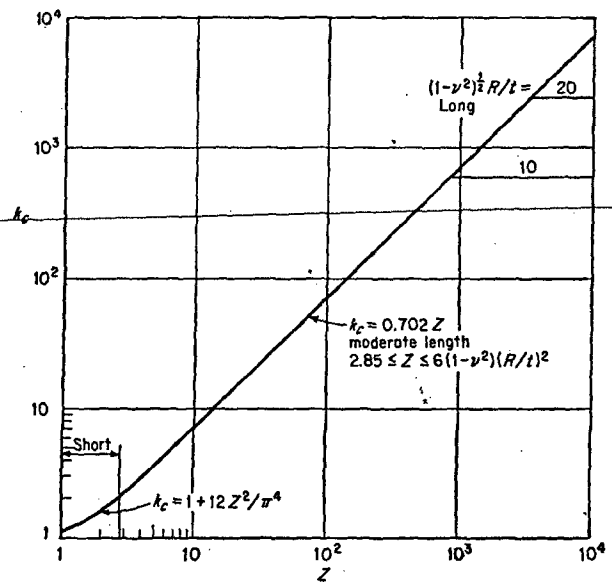

FIG. 8.5. Buckling coefficients for simply supported circular cylinders under axial compression.

length in the loaded axial direction, $m = 1$, and none in the unloaded direction, $n = 0$.

The results given by Eqs. (8.17) and (8.21) are shown in Fig. 8.5. It is to be noted that, at large values of Z, long cylinders buckle as Euler columns with no distortion of the circular cross section. For

cylinders of practical R/t values, however, Euler buckling occurs at values of Z beyond those shown in Fig. 8.5.

8.5. Postbuckling Behavior under Compression

By using the large-deflection equations [Eqs. (7.51) and (7.52)], many investigators have studied the postbuckling behavior of compressed cylinders of moderate length. The essential theoretical results of such an analysis by Donnell and Wan (Ref. 8.7) are shown in Fig. 8.6 for both perfect cylinders and those containing small initial imperfections.

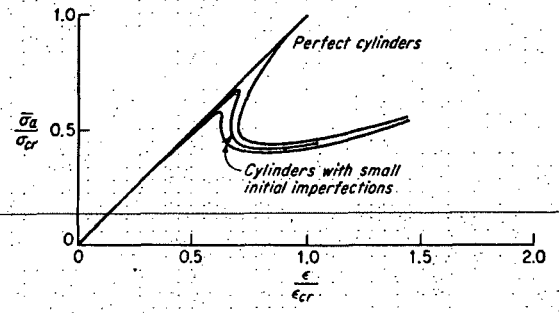

Fig. 8.6. Postbuckling behavior of moderate-length cylinders in axial compression.

It can be seen from Fig. 8.6 that the influence of curvature observed previously in connection with the torsion case is greatly accentuated. For the perfect cylinder under compression, a precipitous decline from the linear buckling stress of Eq. (8.18) occurs after buckling. Of particular importance is the fact that, with continued end shortening, the load-carrying ability is significantly reduced, and it is probably not regained before the onset of plasticity effects.

Cylinders with small initial imperfections exhibit the same type of behavior. Here, too, the postbuckling load-carrying ability apparently does not rise again to the peak load in the region of buckling before the onset of plasticity. As a consequence, we should expect that the failure of moderate-length cylinders in axial compression should be profoundly influenced by the magnitude of the initial imperfections in the cylinder.

This expectation is indeed borne out by the comparison of the linear theory presented in Sec. 8.4 with the large mass of experimental data

on failure of compressed cylinders (Fig. 8.7). It can be observed that none of the test data in the moderate-length region reach the theory and that all are significantly below the theory. Only in the short-cylinder region do the data exceed theory. This is because the test data are for cylinders with clamped ends ($k = 4$ for wide column), whereas the theory is for simply supported ends ($k = 1$ for wide column).

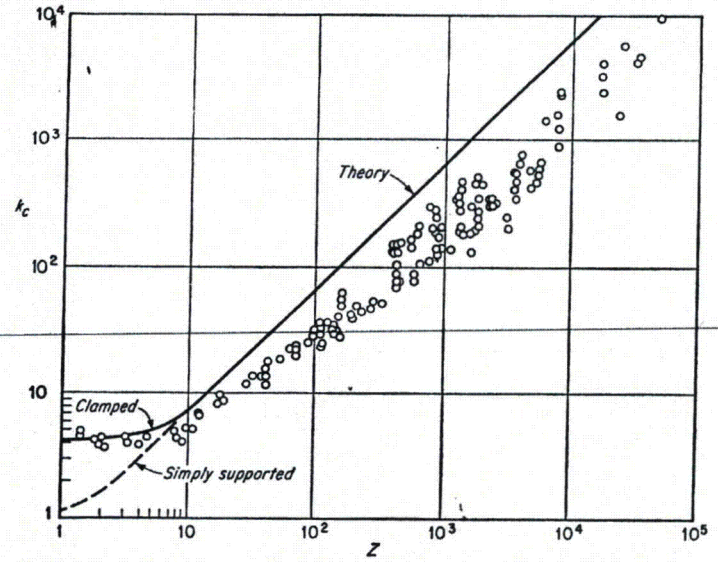

FIG. 8.7. Comparison of linear buckling theory with test data for circular cylinders under axial compression.

At this point, we have reached a rather startling development in that a most significant discrepancy between the results of linear stability theory and experimental data exists. The cause of the discrepancy appears to be associated with the unusual postbuckling behavior of an axially compressed cylinder, and therefore it would seem that we must account for large-deflection effects in this case. Before proceeding to the large-deflection theories that have been developed to resolve this discrepancy, however, we shall first compare the physical behavior of columns, plates, and shells in order to appreciate when large-deflection effects are likely to be of importance.

8.6. Behavior of Compressed Elements

A schematic representation of the postbuckling behavior of axially compressed columns, flat plates, and cylinders is shown in Fig. 8.8 for both theoretically perfect elements and those containing small initial imperfections. It is assumed here that all elements behave elastically.

For the perfect column, the postbuckling behavior is essentially horizontal in the range of end-shortening values considered. The horizontal behavior can be attributed to the fact that, after buckling, no significant transverse-tension membrane stresses are developed to

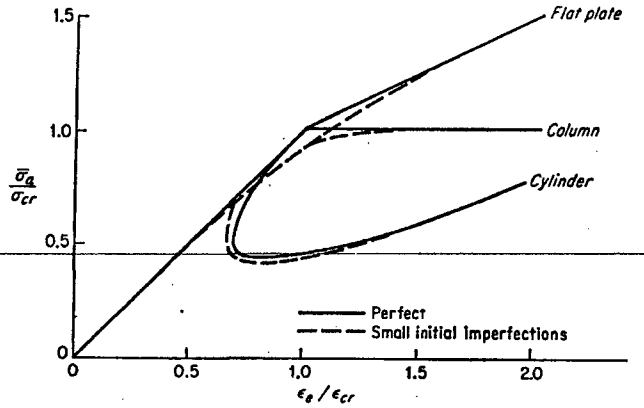

Fig. 8.8. Postbuckling behavior of axially compressed elastic elements.

restrain the lateral motion; therefore, the column is free to deflect laterally under the buckling load.

The flat plate, however, does develop significant transverse-tension membrane stresses after buckling because of the restraint provided by the boundary conditions at the unloaded edges. These membrane stresses act to restrain lateral motion, and thus the flat plate is capable of carrying loads beyond buckling, as indicated in Fig. 8.8.

For the axially compressed cylinder, the effect of the curvature is to translate the postbuckling path considerably downward, with the result that an inward type of buckling is observed to occur. This inward buckling causes superimposed transverse membrane stresses of a compressive nature, so that the buckle form itself is unstable.

As a consequence of the compressive membrane stresses, buckling of an axially compressed cylinder is coincident with failure and occurs

THIS PAGE INTENTIONALLY LEFT BLANK

Tungsten Alloy

THIS PAGE INTENTIONALLY LEFT BLANK

1297 County Line Road, Madison, AL 35756

Date: 8 November 2006

To: Alpha-Omega Services, Inc.
GE Energy

Elevated Temperature Material Characterization

-- Summary of Findings --

Abstract

Summarized herein are the results of specific thermal property tests performed with SD180 as requested by the customer. Elevated temperature tensile testing of this alloy identified a gradual decrease in both offset yield strength and UTS with increasing temperature whereas the elongation at failure rose sharply and then leveled off. Thermal conductivity testing was inconclusive, as thermal testing firms now utilize laser flash diffusivity measurement, which has been shown to provide unreliable results for this material.

Background

ATI Firth Sterling tungsten heavy alloy (WHA) grade SD180 was selected for use in a new large scale design of gamma shield. This alloy has a nominal composition of 95W-3.57Ni-1.43Fe and a nominal density of 18.0 g/cc. The intensity of the gamma flux will result in significant heating of the shield, such that elevated temperature material properties are of significant interest. As a result, this application requires that the shielding material possess a multiplicity of attributes:

- adequate strength and ductility
- good γ radiation attenuation
- sufficient thermal conductivity

The customer specified the tests and the temperatures at which measurements should be made. Temperatures of interest were ambient, 200F, 400F, 600F, and 800F. Further, so as to match the application, testing was to be performed in air. As ATI Firth Sterling is presently equipped only for room temperature material characterization, elevated temperature testing was contracted out to two selected testing firms.

Experimental

Elevated Temperature Tensile Testing

Tensile Testing Metallurgical Lab (Cleveland, OH) was selected to perform the required elevated temperature tests. Tensile testing was conducted using ASTM E8 1" gauge length

specimens pulled at a constant speed of 0.05 in/min. The notch sensitivity of WHA precluded the use of scribe lines or grooves for positioning of a high temperature extensometer. Therefore, crosshead motion was used to generate the displacement measurements in this low compliance, lead screw testing machine. For comparison purposes, a pair of room temperature tensile tests was also performed at ATI Firth Sterling using the same test parameters but with a servohydraulic machine and extensometer. Two specimens were pulled for each test temperature. Averaged results are shown in Table 1.

Table 1. Summary of tensile testing results for SD 180 lot 1808..

Test Temperature	UTS (ksi)	0.2% YS (ksi)	EL (%)
RT (ATIFS)	114.0	93.9	5.0
RT (TTML)	109.7	94.3	3.5
200F (TTML)	112.4	70.8	15.5
400F (TTML)	105.2	60.2	21.8
600F (TTML)	98.2	51.9	21.9
800F (TTML)	95.4	47.8	21.6

The data pairs for each temperature exhibited good agreement, suggesting test results were free from anomalies.

Thermal Property Measurement

Anter Laboratories (Pittsburgh, PA) was selected for measurement of thermal diffusivity and specific heat at the various temperatures of interest. Anter specified that a single disk sample of 0.500" nominal diameter and 0.140" nominal thickness with parallel surfaces and known density be supplied. A SD180 sample from lot 1748 giving a measured ASTM B311 density of 18.11 g/cc was prepared and supplied by ATIFS. Measurements were conducted per ASTM E1461-01. Results are presented in Table 2.

Table 2. Summary of thermal property evaluation of SD 180 lot 1748.

Test Temperature		Diffusivity	Specific Heat	Conductivity
Nom. (F)	Actual (C)	(cm^2/sec)	(J/(kg-K))	(W/m-K)
RT	25	0.2742	154.7	76.8
200	97	0.2700	159.2	77.8
400	206	0.2624	163.4	77.6
600	316	0.2553	170.3	78.8
800	427	0.2451	173.9	77.2

The thermal conductivity remained relatively constant over the entire test temperature range, whereas specific heat showed a gradual increase and thermal diffusivity a slow decrease. The room temperature density was applied to all conductivity calculations, as the very low CTE of WHA (less than 5.0×10^{-6} K^{-1}) would result in a change of calculated value of only 0.5 W/m-K or less even at the highest test temperature. This was a factor of 4 less than the reported uncertainty of the test procedure.

Discussion of Results

In reviewing the tensile data set generated, the most pronounced effect was that of moving above the ductile to brittle test temperature (DBTT) for WHA, which in most metallurgical conditions is in the vicinity of room temperature. This accounts for the significant increase in alloy ductility, as measured by %EL. Accompanying this increase in ductility was a gradual decrease in both the ultimate and offset yield strengths, which is to be expected in light of induced thermal effects on various dislocation mechanisms that determine deformation response under load. These effects can be seen clearly when the data of Table 1 are plotted and displayed in Figure 1.

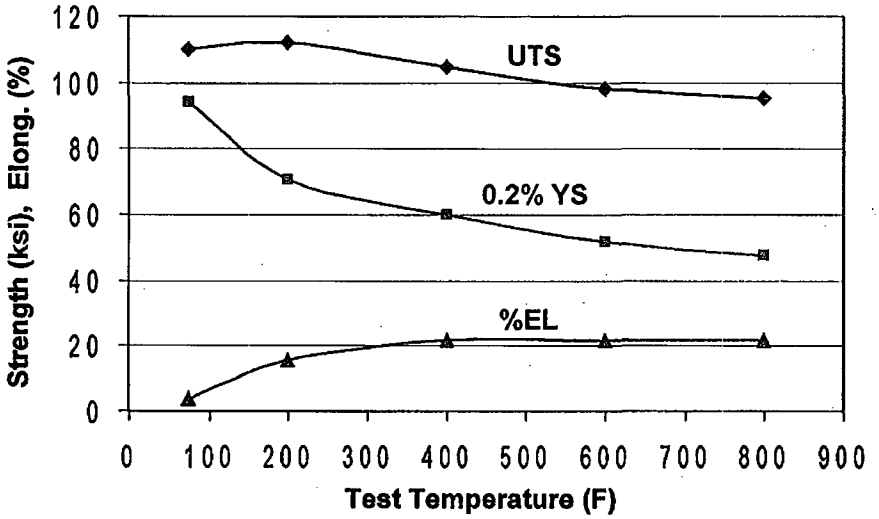

Figure 1. Graphical display of tensile property variation with test temperature.

While the strength of the gamma shield would decrease slightly with heating, the durability of the shield would tend to increase, depending on the magnitude of temperature rise attained.

The data set obtained from thermal property evaluation exhibited consistent trends. However, the resultant calculated values for thermal conductivity, which averaged 78 W/m-K, were well below the accepted industry values for this composition class of WHA. The literature for about two decades has reported values in the range of 110-130 W/m-K. This range is much more in keeping with an alloy having 95 wt.% of a metal that has a conductivity of ~160 W/m-K and is present as a virtually pure phase in the two phase WHA microstructure. The reason for the low measured values is presently unknown. The results obtained appear to underestimate the accepted thermal conductivity by about 35%. Dialogue with Anter revealed no apparent test execution problems. The data set obtained from Anter Laboratories did show that for the temperature range of interest, the thermal conductivity of the WHA, though of systematically low magnitude, did not vary significantly. It was decided that a second independent test be conducted in an effort to understand these results relative to industry accepted values.

Supplemental Testing

In view of the question posed from thermal conductivity testing of the SD180 alloy, a second test sample was prepared for submission to a different laboratory for analysis. While

Anter is nationally recognized for both thermal analysis and the manufacture of thermal analyzers, it was desirable to have a completely independent measurement made. Raul Pomares forwarded the firm of M & P Lab, in that they performed thermal measurements for GE Energy in the past. However, when their thermal analysis contact M. B. Bolduc was contacted, it was learned that they do not perform any thermal conductivity measurements. Harrop likewise, while performing other thermal measurements, does not perform conductivity measurement. Netzsch was therefore chosen as the second source for SD180 thermal conductivity measurement. Netzsch indicated that they also use the laser flash method per ASTM E1461 and calculate the thermal conductivity from measured diffusivity. After about a 6 week lead time, the room temperature test was completed and is shown in Table 3. Netzsch used a density of 18.0 g/cc for the calculation, whereas our measurement yielded 18.06 g/cc.

Table 3. Second conductivity evaluation of grade SD 180.

Test Temperature		Diffusivity	Specific Heat	Conductivity
Nom. (F)	Actual (C)	(mm^2/sec)	(J/(g-K))	(W/m-K)
RT	25	16.6	0.153	45.9

This new value for thermal conductivity was even further away from the expected value based on composition and density. This measurement underestimated the accepted average conductivity by at least 60%. After obtaining this margin of error, testing was halted, as any elevated temperature values would likewise be of no value.

Conclusions

The selected elevated temperature characterization of SD180 provided a more comprehensive prediction of alloy performance in the target application. The identified property trends were in keeping with fundamental elevated temperature response of metallic materials. Excellent ductility was retained over the entire range of test temperature.

Thermal conductivity measurements however were inconclusive. Two independent tests – both using nationally recognized testing firms that not only routinely perform toll thermal testing but also actually manufacture the equipment – failed to provide results that were even in approximate agreement or close to the accepted values used for decades within the refractory metals industry. These low values should therefore be disregarded, as they cannot be independently repeated. As the entirety of this testing was conducted off site, the reasons for this extreme variation in measurements are presently unknown. Both testing houses guarantee conformance to ASTM E1461. Whatever the case, those skilled in performing laser flash tests have not demonstrated that this technique, now used almost universally for thermal conductivity measurements, is appropriate for tungsten heavy alloy. To the contrary, conductivity measurements obtained to date suggest the flash diffusivity approach is unreliable for this material. The higher industry accepted values of 110-130 W/m-K were no doubt made by techniques that predated laser flash diffusivity and measured conductivity directly using larger size samples. No presently available source for repeating earlier test methods is known.

S. G. Caldwell
Technical Director – Tungsten Alloys

Firth Sterling
ATI Engineered Products

1297 County Line Road, Madison, AL 35756 256-464-7738 scaldwell@atimwp.com

4 September 2008

Troy Hedger / Raul J. Pomares
Alpha-Omega Services, Inc.
9156 Rose Street
Bellflower, CA 90706

Dear Troy / Raul:

I have prepared the following comments in response to your request to address the differences between our previously reported data (under Alpha-Omega Services P.O. #AOS-03590) and the cited specific heat values listed in NUREG/CR-6150.

In briefly revisiting previously submitted project reports, the initial thermal analysis data presented as part of our 7 September 2006 report contained a *Transmittal of Test Results* document from Anter Laboratories, a leading thermal analysis equipment manufacturer and provider of toll thermal analysis services. Testing of our tungsten heavy alloy grade SD180 material used in work defined by the referenced AOS purchase order was conducted by laser flash measurement, as described by ASTM E1461-01 using NIST traceable standards in a NADCAP certified laboratory. This testing house was extremely well qualified to make accurate measurements of specific heat.

Data were obtained at 5 temperatures of interest. The following values were reported by Anter for the 18.1 g/cc density tungsten heavy alloy (nominal composition 95W-3.57Ni-1.43Fe):

Nominal Temperature (F)	Specific Heat (J/[kg-K])
RT	154.7
200	159.2
400	163.4
600	170.3
800	173.9

Then, at a later date, additional thermal analysis of a SD180 sample was performed by Netzsch, who is also both a manufacturer of thermal analysis equipment as well as a toll service provider. As our 11 December 2006 report detailed, Netzsch obtained the following result using the same laser flash ASTM E1461 technique:

Nominal Temperature (F)	Specific Heat (J/[g-K])
RT	0.153

1

When the reported unit of measure is converted from a gram to kilogram basis, this supplemental testing by a second independent testing house yielded excellent agreement in specific heat – a value of 153 compared to the earlier 154.7 (J/[kg-K]). These values were thus in agreement within ~1.1% - an excellent match for single test data comparison.

In examining Section 15 of NUREG/CR-6150, it is not surprising to find disagreement in specific heat values to those we reported – it is rather to be expected. Tables 15-1 and 15-2 both list date for pure, elemental tungsten (W) – not tungsten heavy alloy. The SD180 alloy additionally contains Fe and Ni, and possesses a lower theoretical alloy density that pure W.

The relevance of previously reported specific heat values for the SD180 used in the aforementioned project over those contained in the cited NUREG document can therefore be summarized as follows:

1. NUREG/CR-6150 does not even relate to the tungsten heavy alloy used in the cask project.
2. NUREG/CR-6150 contains calculated values only, whereas our reported values were from actual material testing conducted by equipment manufacturers to an ASTM standard.
3. The thermodynamic data used for computation of NUREG/CR-6150 data are not given in Section 15. Even for the case of pure W, the calculated density reported in NUREG/CR-6150 Section 15.3 is 19.600 g/cc, which is greater than the tungsten industry accepted value of 19.3 g/cc for W as well as the value of 19.30 g/cc specified in the National Institute of Standards Physical Reference Data listing. It would appear that at least that input datum used in thermal calculations is in slight error even for the case of pure W. Calculated data are only as good as the input data and model.
4. Specific heat values we reported previously accounted for the actual measured density of the SD180 tungsten heavy alloy, as was determined using ASTM B311. As both chemical makeup and density varied from that of pure W, it is only natural that the thermal properties would differ from pure W as well.
5. The values we reported from Anter and Netzsch tests are consistent in trend with data for pure W in Table 15-1 of NUREG/CR-6150. For example, room temperature specific heat for pure W is listed as ~138 J/(kg-K), whereas testing of SD180 gave ~155 J/(kg-K) – an increase of ~12%. The tungsten heavy alloy contained 5 wt.% of transition metals having significantly higher specific heats than W (~460 J/(kg-K) for Ni, ~440 J/(kg-K) for Fe). It is therefore only expected that the room temperature specific heat for the SD180 heavy alloy would be higher than that of pure W.

There is therefore no reason whatsoever to question the specific heats reported by ATI Firth Sterling for SD180 based on NUREG/CR-6150. At best, the cited Section 15 data are not applicable for the reasons described above. Please contact me if further information is needed.

Yours truly,

Steven G. Caldwell

Steven G. Caldwell, Ph.D.
R&D Director
ATI Firth Sterling
1297 County Line Road
Madison, AL 35756

Tungsten Heavy Alloy

Engineering Manual

S. G. Caldwell, PhD

ATI Firth Sterling
1297 County Line Road
Madison, AL 35756
ph 888-778-0979
fax 888-208-9109

www.firthsterling.com

2. Alloy Selection Criteria

Density

Density is the single most important property that makes a WHA the material of choice for virtually all applications. The selection of a specific composition for a given density application may ultimately be made on the basis of mechanical property requirements in conjunction with sintering considerations, unless a density is mandatory.

As is true with most mechanical designs, the optimum design is the one that adequately addresses all critical parameters and offers the best compromise of the remaining options. As the density of a WHA is increased, the available ductility decreases. Alloy density varies according to tungsten content, as can be seen in the following table of ATI Firth Sterling standard alloys. These alloys conform to the various classes as defined by industry standard MIL-T-21014D (alternately AMS-T-21014 and ASTM B777).

Grade Specification Conformance

Alloy*	Nom. Composition (Wt. %)	MIL-T-21014D Classification	Typical Density (g/cc)	Typical Density (lbs/in^2)	Magnetic Permeability (μ)
SD170	90W-7.14Ni-2.86Fe	Class 1	17.09	0.618	5.0-5.5
Dens21	89.8W-8.92Ni-1.28Fe	Class 1	17.16	0.620	<1.01
SD175	92.5W-5.36Ni-2.14Fe	Class 2	17.62	0.637	4.5-5.0
Dens23	92.5W-6.56Ni-0.94Fe	Class 2	17.67	0.639	<1.01
SD180	95W-3.57Ni-1.43Fe	Class 3	18.12	0.655	4.0-4.5
Dens25	95W-4.37Ni-0.63Fe	Class 3	18.16	0.656	<1.01
SD185	97W-2.14Ni-0.86Fe	Class 4	18.56	0.671	1.6-2.0

Dens21 is manufactured with a tungsten content slightly under the nominal in order to have a sintered density positioned more centrally within the defined interval. In addition to these standard compositions, ATI Firth Sterling can also manufacture custom alloys.

Mechanical Properties

Mechanical properties of modern WHAs far surpass those available from WHAs even a few decades ago. Three factors primarily contribute to this advance: (1) higher purity raw materials, (2) cleaner and more precisely controlled process environments, and (3) the use of modern tungsten-nickel-iron (W-Ni-Fe) compositions rather than the older alloys containing copper.

It is also important to note as a general consideration that the maximum attainable property set for these alloys varies with the size of the blank. This is a direct consequence of the nature of the sintering operation used to make the parts. A number of gradients – thermal, chemical, and gravitational – exist during sintering. As the maximum section thickness of a given part is increased, thermochemical removal of impurities from the center of the pressed part prior to surface pore closure becomes more difficult. Therefore, small parts will always tend to have higher mechanical properties than larger ones.

As seen in the table below, the nominal properties listed meet or exceed the industry standard requirements. All values shown are for material in the as-sintered state, as this is the most commonly supplied condition of the material for commercial applications.

Typical Densalloy™ Properties

Alloy*	Wt.% W (nominal)	UTS (ksi)	0.2% YS (ksi)	EL (%)	Elastic Modulus (x 10^6 psi)	Hardness (HRC)
SD170	90	120	80	10	45	28
Dens21	90	110	75	4	45	28
SD175	92.5	120	80	8	48	28
Dens23	92.5	110	80	3	48	28
SD180	95	120	75	6	50	29
Dens25	95	110	75	3	50	29
SD185	97	110	75	2	52	30

All WHAs are susceptible to hydrogen embrittlement, which lowers the ductility of the alloy. ATI Firth Sterling can provide alloys in a hydrogen outgassed condition, which in some cases can double the tensile elongation. Further property enhancement is possible through additional post-sinter processing.

For structural (load bearing) applications, it is recommended that alloy be used in the most ductile condition feasible for the given part. This promotes "bend before break" behavior needed for critical parts. Part durability is favored by use of lower tungsten content Class 1 and 2 alloys such as SD170 and SD175.

Thermal and Electrical Properties

The properties of WHA are governed by the properties of its principal constituent, tungsten. While properties will vary slightly with tungsten content, binder composition, and microstructure, several example properties will be cited for SD180, as it is near the middle of the commercially defined compositional range.. The thermal conductivity of the alloy is ~80 W/m-°K and a corresponding electrical conductivity of ~13% IACS. The thermal expansion is very low, with a CTE of only ~5.0E-6/°C at 20°C – only about 1/3 that of ferrous alloys. The specific heat of SD180 at room temperature is ~0.037 cal/g-°C. While the melting point of pure tungsten is extremely high, WHAs will begin to form a liquid phase when heated in excess of ~1450°C (2642°F). Therefore, unlike pure W, WHAs are not suitable for high temperature applications.

The change in tensile properties of WHA at elevated temperature is of increasing interest to oilfield engineers. As drilling depths approach 5 miles, there is growing interest in the ability of WHA components to survive the harsh pressure and elevated temperature conditions. The following graph shown below illustrates the systematic change in mechanical properties with temperature for vacuum annealed SD175 typical of what that industry uses. For applications in which the service temperature will exceed ~300°C, slight surface oxidation will occur in air. A protective atmosphere should be considered for prolonged exposure at or above this temperature. It is important to note that at service temperatures exceeding ~500°C – beyond the range of the data shown below – WHA

THIS PAGE INTENTIONALLY LEFT BLANK

Tungsten

Properties, Chemistry, Technology of the Element, Alloys, and Chemical Compounds

Erik Lassner and
Wolf-Dieter Schubert
Vienna University of Technology
Vienna, Austria

Kluwer Academic / Plenum Publishers
New York, Boston, Dordrecht, London, Moscow

Library of Congress Cataloging-in-Publication Data

Lassner, Erik.
Tungsten : properties, chemistry, technology of the element, alloys, and chemical compounds / Erik Lassner and Wolf-Dieter Schubert.
p. cm.
Includes bibliographical references and index.
ISBN 0-306-45053-4
1. Tungsten. I. Schubert, Wolf-Dieter. II. Title.
QD181.W1L37 1998
620.1'8934--dc21 98-45787
CIP

ISBN 0-306-45053-4

10 9 8 7 6 5 4 3 2 1

A C.I.P. record for this book is available from the Library of Congress.

Significant strengthening is observed up to 2700 K (2427 °C). Above this, rapid particle coarsening occurs, and the strengthening effect fades. Additions of rhenium provide ductility at low temperatures by decreasing the DBTT.

W–Re–HfC alloys cannot be produced by powder metallurgical techniques owing to the high oxygen affinity of hafnium. They are produced by arc melting.

Yield strength and ultimate tensile strength of a W–3.6Re–0.26HfC alloy as a function of temperature are shown in Fig. 6.12, in comparison to pure W, W–3.6Re, and W–3.6Re–1ThO_2.

W–Re–HfC alloys are the strongest man-made metallic materials at temperatures above 2000 K [6.25].

6.3. TUNGSTEN COMPOSITES

Tungsten metal exhibits outstanding thermal properties, which makes it attractive for a broad range of applications. However, for certain applications, its electrical and thermal conductivity, sensitivity toward oxidation, and poor workability are unsatisfactory. These limitations have led to the development of two-phase alloys, in which the useful properties of tungsten are combined with those of the additive.

Two important alloy systems belong to this group and are described below:

- The so-called heavy metal alloys, based on W–Ni–Fe and W–Ni–Cu–(Fe). They are used wherever high density, excellent mechanical properties, and good workability are required.
- W–Cu and W–Ag alloys, in which the high electrical and thermal conductivity of copper or silver is combined with the high hardness and wear resistance of tungsten.

6.3.1. Tungsten Heavy Metal Alloys [6.1, 6.2, 6.26, 6.27, 6.29]

The term *tungsten heavy metal* or *heavy metal* is used for a group of two-phase composites, based on W–Ni–Fe and W–Ni–Cu. They are characterized by a high density and a novel (unique) combination of strength and ductility.

Tungsten is the main component of the alloys (typically present in the range of 90 to 98 wt%) and the reason for their high density (between 17 and 18.5 g/cm^3). Nickel, iron, and copper serve as a binder matrix, which holds the brittle tungsten grains together and which makes the alloys ductile and easy to machine. A typical microstructure is shown in Fig. 6.13. It consists of spherical tungsten grains (20 to 60 μm in diameter), which are embedded in a tough, metallic matrix. While the grains are nearly pure bcc tungsten, the fcc binder matrix contains about 20 wt% W in solid solution.

Heavy metals are used for applications, where the high specific weight of the material plays an important role. They are used as counterweights, rotating inertia members, X-ray and γ-radiation shields, as rigid tools for machining, as well as for defense purposes (kinetic energy penetrators, fragmentation devices, etc.).

Fabrication [6.26, 6.27]. Heavy metals are produced by conventional P/M techniques. A flow chart of the fabrication process is shown in Fig. 6.14. Elemental powders (W,

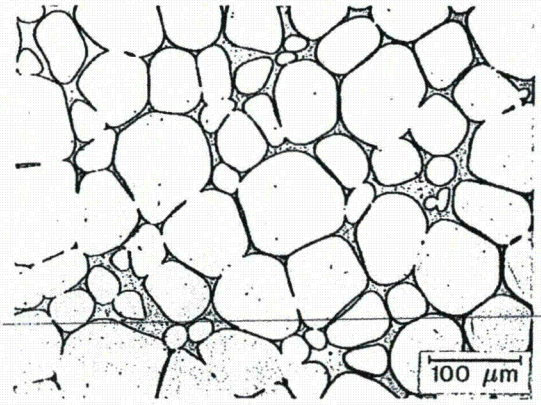

FIGURE 6.13. Optical micrograph of a 95 wt% tungsten heavy metal alloy with 3.2 wt% Ni and 1.8 wt% Cu. By courtesy of Plansee AG, Reutte, Austria.

Fe, Ni, Cu) are blended in mixers or ball mills to the desired ratio, compacted to form a green body, and subsequently liquid-phase sintered. Assuming proper manufacturing conditions, they exhibit full or near-theoretical density in the as-sintered condition.

Powder particle sizes are in the range of 2 to 6 μm. Both die pressing and isostatic pressing (dry- and wet-bag pressing) are in use. No lubricant is commonly added, since the green strength is high enough to handle the compacts. Powder injection molding (PIM) is used for applications where net shaping is desired and large quantities of complex parts are produced [6.28].

Sintering is commonly carried out in molybdenum-wire resistance-heated furnaces under hydrogen or nitrogen mixtures (dissociated ammonia) but can also be performed in vacuum units. The use of wet hydrogen has become industrial practice to suppress hydrogen embrittlement (water vapor porosity) [6.29]. The temperature/time program of the sintering cycle must be adjusted to the composition and size of the sintered parts. A

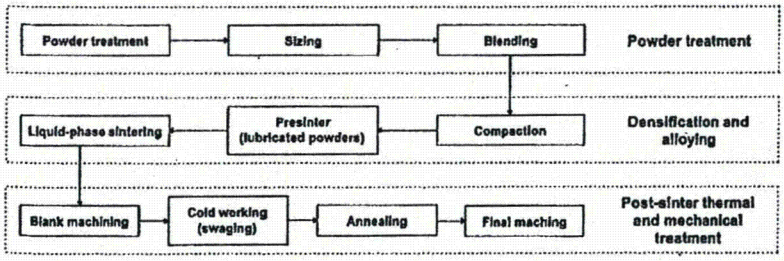

FIGURE 6.14. Flowchart of the fabrication process of tungsten heavy metal penetrators [6.26].

cleaning step in hydrogen at 1000 °C is commonly performed to render the outgassing of volatile compounds. High-purity powder grades must be used for sintering. Otherwise, blistering will occur on liquid-phase sintering, and interface precipitations will occur on cooling.

Isothermal sintering is carried out above the eutectic temperature, typically between 1440 and 1500 °C, but can be as high as 1600 °C. The higher the tungsten content of the alloy, the higher the temperature. Tungsten–nickel–copper alloys are sintered at somewhat lower temperatures than tungsten–nickel–iron alloys. Sintering times are between 30 minutes and two hours. Prolonged sintering under dry hydrogen leads to swelling of the parts and significant embrittlement due to pore coarsening by Ostwald ripening and coalescence. Residual porosities larger than 0.5% drastically reduce the ductility [6.30, 6.31].

On cooling, a significant amount of tungsten remains in solid solution, depending on the binder composition and the cooling rate. The solubility is highest in binary W–Ni alloys (up to 40 wt%; resulting in low ductility), but additions of Fe and Cu depress it to lower values (typically 20 to 25 wt% W), providing a tough and ductile binder matrix.

Shrinkage porosity can form on cooling, in particular in W–Ni–Cu alloys and at high cooling rates; furthermore, impurities (P, S, C) segregate at the tungsten matrix interface. Both effects must be controlled by proper manufacturing conditions, since they significantly lower the ductility.

Optimal mechanical properties require subsequent heat treatment of the alloys. Solution annealing at 900 to 1300 °C and subsequent quenching to avoid impurity segregation and formation of intermetallic phases significantly improves ductility [6.26]. Heavy metals can be cold-worked (swaged, rolled) to increase hardness and strengths at the expense of elongation and toughness. Aging at 500 °C after 25% deformation (cold work) is a compromise to achieve both high ultimate tensile strengths and elongation. Conventional procedure is a double swaging–heat treatment cycle (deformation 25–30%) [6.32]. The structure shows that the original spheroids formed during liquid-phase sintering have been transformed to ellipsoids on deformation (Fig. 6.15). Recently, the advantage of large deformation levels (up to 95%) yielding in a fibrous microstructure (Fig. 6.16) has been demonstrated [6.32]. Heavy metals exhibit a ductile-to-brittle transition temperature. In comparison to pure tungsten it is, however, not a sharp transition but spreads over several hundred degrees [6.1].

Although a considerable amount of densification already occurs during solid-state heating, isothermal liquid-phase sintering is a prerequisite to obtain near-theoretical density and a high degree of microstructural homogeneity. Rapid final densification occurs on formation of the liquid phase under the action of capillary forces. Particle rearrangements, solution/reprecipitation processes (Ostwald ripening), and coalescence contribute to a higher packing density and a significant grain coarsening during sintering. The original tungsten powder grain size of 3–5 μm is transformed during sintering to rounded tungsten particles (spheroids) of at least 10 times the original grain diameter. Shape accommodation (formation of polyhedras with rounded corners) plays an important role in high tungsten alloys, where only a small quantity of liquid is available for achieving full density.

Depending on the binder composition, heavy metals can be classified into two main groups [6.2, 6.27]:

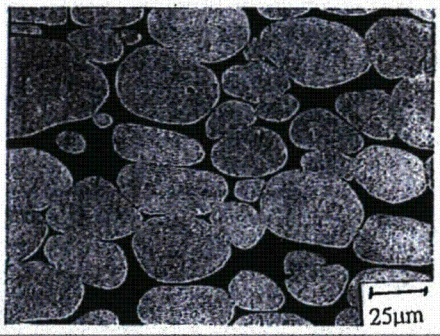

FIGURE 6.15. Microstructure of a W–Ni–Fe–Co alloy after swaging by 30% [6.32]. By courtesy of A. R. Bentley, M. C. Hogwood, and M. Power, Defence Research Agency, Kent, England.

(a) W–Ni–Fe (Ni: 1–7 wt%, Fe: 0.8–3 wt%, Mo: 0–4 wt%)

This group is ferromagnetic. Typical nickel-to-iron ratios range between 1:1 and 4:1. The preferred ratio is 7:3, since this composition avoids the formation of intermetallic phases [6.26]. W–Ni–Fe alloys exhibit excellent strength/ductility combinations and can be cold-worked to a reduction of 60% without intermediate annealing. Molybdenum acts as grain refiner. Higher additions of iron and/or additions of molybdenum cause a significant matrix-strengthening effect and improve high-temperature strength (Gyromet grades) [6.2]. Other additives, such as Co, Ta, and Re, act as grain refiners and increase hardness and strength, but lower the ductility [6.29]. Rhenium additions are of interest in net-shape production, since their high strength in the as-sintered condition (1180 MPa) does not require any post-sintering treatment [6.33].

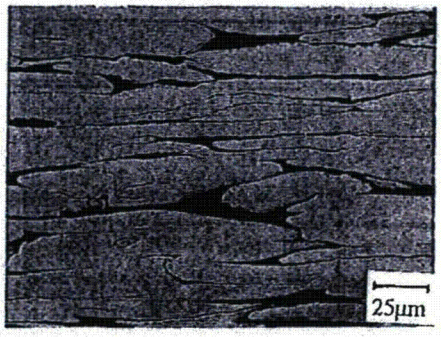

FIGURE 6.16. Microstructure of a W–Ni–Fe–Co alloy after deformation by 80% [6.32]. By courtesy of A. R. Bentley, M. C. Hogwood, and M. Power, Defence Research Agency, Kent, England.

(b) W–Ni–Cu (Ni: 1–7wt%, Cu: 0.5–3 wt%, Fe: 0–7 wt%)

Members of this group are nonmagnetic and exhibit a higher electrical conductivity. The nickel-to-copper ratio ranges from 3:2 to 4:1. W–Ni–Cu alloys exhibit lower strength and ductility than comparable W–Ni–Fe alloys. Due to the low melting point of copper, low heating rates are required to obtain full density.

Properties: [6.1, 6.34, 6.35]. Some properties of tungsten heavy metal alloys are summarized in Table 6.1. Ultimate tensile strengths (660–1350 MPa), yield strengths (565–300 MPa), and fracture elongations (5–30%) can vary widely. In general, mechanical properties are very sensitive to processing conditions, impurities, and microstructure. Problems with controlling porosity, impurities, and microstructural homogeneity are therefore common in heavy alloy fabrication [6.31]. Residual sinter porosity and the formation of interface precipitates are the main reason for inferior material properties.

With increasing tungsten content, the contiguity of the tungsten grains increases (i.e., the W–W interfacial area as a fraction of the total interface area) and both strength and ductility decrease [6.36]. This "microstructural limitation" of the properties is demonstrated in Fig. 6.17 for alloys of different tungsten contents [6.1, 6.31, 6.37]. While the

TABLE 6.1. Properties of Tungsten Heavy Metal Alloys[a]

Properties	1	2	3
Density ($g \cdot cm^{-3}$)	17.0–18.5	17.0–18.5	17.1–18.6
Young's modulus (GPa)	350–400	320–380	—
Shear modulus (GPa)	—	125–160	—
Poisson's ratio	0.28–0.29	0.28–0.29	—
Hardness			
HV10	270–360	270–470	—
HB30	—	250–450	—
RC	—	—	28–40
Tensile strength (MPa)			
20°C	870–1000	660–1350	880–1320
100°C	—	560–730	—
500°C	340–650	340–610	—
1000°C	220–260	90–260	—
Yield strength (0.2%) (MPa)	600–700	565–1300	750–1240
Fracture elongation (%)	10–30	—	5–30
Compressive strength (MPa)	3500–4500	3500–5500	—
K_{Ic} ($MPa \cdot mm^{-1}$)	800–6300	—	—
Compressibility (% of length)	—	—	45–60
Charpy value (notched)	0.9–2.8	—	—
Specific electrical resistivity ($\mu\Omega \cdot m$)	0.10–0.18	0.10–0.18	—
Mean linear coefficient of thermal expansion at 20–800°C ($mm^{-1} \cdot K^{-1}$)	$5.2–6.5 \times 10^{-6}$	$5.2–6.5 \times 10^{-6}$	—
Half-value thickness			
against ^{60}Co	—	8.5–9.7	—
against ^{137}Cs	—	4.5–5.2	—

[a] 1. Pink and R. Eck, "Refractory Metals and their Alloys," in: *Materials Science and Technology* (R. W. Cahn, P. Haasen, and E. J. Kramer, eds.), Vol. 8, pp. 591–638, VCH, Weinheim, (1996).
2. Metallwerk Plansee, Densimet Schwermetall Legierungen, Company Brochure, Reutte, Austria (1982).
3. Ashot Ashkelon, Tungsten-Based Products, Company Brochure.

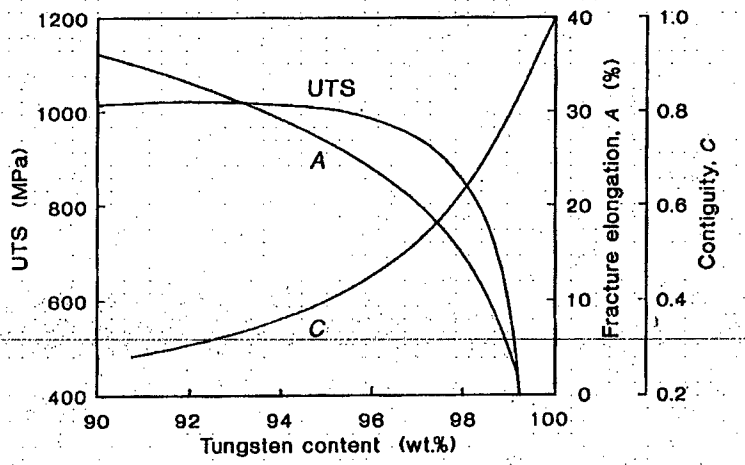

FIGURE 6.17. Optimum values of room-temperature strength and fracture elongation and their correlation with the contiguity factor for tungsten heavy alloys [6.1, 6.31].

trend is most pronounced for the fracture elongation, the tensile strength exhibits a maximum at about 85 vol% W (93 wt%) before it significantly decreases. At 99 wt% W, the elongation is zero and the tensile strength is about 400 MPa [6.38].

Recently, it was demonstrated that large deformation levels yield exceptionally high tensile strength levels (up to 1700 MPa), combined with fracture elongations above 15% [6.32].

Besides the high density and the unique combination of high strength and ductility, there are other attributes which make heavy metals a versatile product:

- the high modulus of elasticity (much higher than steel),
- excellent vibration damping characteristics (for chatter-free heavy machining),
- its good machinability,
- the high absorption ability for X-rays and γ-rays,
- good thermal and electrical conductivity,
- low electrical erosion and welding tendency,
- good corrosion resistance.

Research in tungsten heavy alloys was previously boosted by the ballistic application as anti-amor kinetic energy penetrator. Numerous papers have appeared in the last years and reviews have recently been published [6.29, 6.39, 6.40]. Although the basic requirements are the same for civil as for defense applications (i.e., high density, strength, and elongation), there are two more important factors which must be considered for this specific application: the behavior of the material under high strain rate conditions and their ballistic performance (i.e., their penetration ability). In particular, the latter aspect is of critical importance and, to a certain extent, still a weak point of heavy metals. Their ballistic performance is inferior compared to depleted uranium, which is still used as a

standard penetrator material [6.29]. Nevertheless, recent environmental considerations have put a strong emphasis on substituting depleted uranium by heavy metals because of its radioactivity. Efforts to improve the ballistic performance through proper processing and compositional modifications have failed [6.29, 6.39]. Recent research has therefore focused on alternative matrix alloys, such as tungsten–hafnium, tungsten–uranium composites [6.29], or heavy metal alloys with a spiculating core of WC [6.41].

6.3.2. *Tungsten Copper and Tungsten Silver* [6.1, 6.2, 6.42].

Tungsten–copper and tungsten–silver composites are widely used in mechanical and electrical engineering. Typical applications include high-, medium-, and low-voltage circuit breakers (W–Cu, W–Ag), resistance welding electrodes, electrode materials for electrical discharge machining, and heat sink materials for microelectronic packaging (W–Cu). More recently, W–Cu composites have been tested as heat flux components in experimental fusion reactors [6.43] and as materials in MHD (magnetohydrodynamics) power generation systems [6.44].

They combine the high hardness, hot strength, and wear resistance of tungsten with the outstanding electrical and thermal conductivity of the two high-conductivity metals. Furthermore tungsten increases the resistance of the materials against spark and arc erosion (burn-off) and lowers the sticking and welding tendency, which are both important criteria for heavy-duty electrical contacts, where switching currents can be up to 100 kA and arc temperatures of a few 10,000 K can occur within a few milliseconds [6.45]. Under arcing conditions, the contacts are cooled through the melting and evaporation of silver or copper ("transpiration" cooling), an effect which was earlier used for rocket nozzle throat liners (for example for underwater-launched ballistic missiles) made of W–Ag [6.2].

W–Cu and W–Ag composites are not real alloys in the strict meaning of the word, because the mutual solubility of the components is practically zero. Therefore, they are also sometimes called "pseudoalloys."

Production. Powder metallurgy is the only viable way to produce composites of high quality. The method of production depends on the composition ratio. Materials with 10 to 40 wt% copper (20 to 50 wt% silver) are commonly produced by infiltration, while at higher copper or silver contents the powders are blended, pressed, and subsequently solid-state sintered [6.42, 6.46].

Infiltration of porous structures. A porous tungsten skeleton is first produced by pressing either pure tungsten powder or a mixture of tungsten powder and small amounts of the additive element with subsequent sintering in a reducing atmosphere at comparably low temperatures (1200–1800 °C). The porosity of the compact can be varied by the pressing and sintering parameters, as well as by the grain size distribution of the starting tungsten powder. It determines the percentage of infiltrate. For higher copper and silver contents, loose tungsten powder can also be infiltrated.

Infiltration is accomplished by immersion, dipping, or flooding, either in vacuum, inert gas, or, preferably, in reducing atmosphere at 1150–1250 °C. Oxide layers disturb the infiltration process and must be removed prior to infiltration by reduction with hydrogen. Trace impurities can impair the wetting between tungsten and the melt (for example, silicon) but can also improve it (nickel, cobalt, iron) [6.47]. Densities of 96% up to near-

FIGURE AND TABLE NO. 68R. RECOMMENDED VALUES FOR THERMAL LINEAR EXPANSION OF TUNGSTEN W

RECOMMENDED VALUES

T	$\Delta L/L_0$	$\alpha \times 10^6$
[Temperature, T, K; Linear Expansion, $\Delta L/L_0$, %; α, K^{-1}]		
5	-0.086	0.0006
25	-0.086	0.21
50	-0.085	0.68
100	-0.076	2.6
200	-0.040	4.1
293	0.000	4.5
400	0.048	4.5
500	0.093	4.6
600	0.140	4.7
700	0.188	4.8
800	0.237	5.0
900	0.287	5.0
1000	0.339	5.2
1200	0.444	5.3
1400	0.551	5.4
1600	0.661	5.6
1800	0.774	5.8
2000	0.893	6.1
2200	1.020	6.6
2400	1.157	7.1
2600	1.307	7.8
2800	1.469	8.3
3000	1.646	9.2
3200	1.837	10.0
3400	2.042	10.8
3600	2.263	11.6

REMARKS

The tabulated values are considered accurate to within ±5% over the entire temperature range. These values can be represented approximately by the following equations:

$\Delta L/L_0 = 4.266 \times 10^{-4} (T - 293) + 8.479 \times 10^{-8} (T - 293)^2 - 1.974 \times 10^{-11} (T - 293)^3$ $(293 < T < 1395)$

$\Delta L/L_0 = 0.548 + 5.416 \times 10^{-4} (T - 1395) + 1.952 \times 10^{-8} (T - 1395)^2 + 4.422 \times 10^{-11} (T - 1395)^3$ $(1395 < T < 2495)$

$\Delta L/L_0 = 1.226 + 7.451 \times 10^{-4} (T - 2495) + 1.654 \times 10^{-7} (T - 2495)^2 + 7.568 \times 10^{-12} (T - 2495)^3$ $(2495 < T < 3600)$

General Plastics LAST-A-FOAM

THIS PAGE INTENTIONALLY LEFT BLANK